Sampled-data based discrete and fast load frequency control for power systems with wind power

Xingchen Shang-Guan[a,b,c], Yong He[a,b], Chuanke Zhang[a,b], Lin Jiang[c,*], Joseph William Spencer[c], Min Wu[a,b]

[a]*School of Automation, China University of Geosciences, Wuhan 430074, China*
[b]*Hubei Key Laboratory of Advanced Control and Intelligent Automation for Complex Systems, Wuhan 430074, China*
[c]*Department of Electrical Engineering and Electronics, University of Liverpool, Liverpool L69 3GJ, United Kingdom*

Abstract

Load frequency control employs communication networks to transmit measurements and control signals. The controller is usually designed in continuous-mode and discretized in implementation with a large sampling period, which may result in a degraded dynamic performance or even cause system instability. On the other hand, high penetration of wind power reduces the inertia of the power system, leading to a faster frequency response and larger frequency deviation after a contingency, and desires a fast load frequency control. Therefore, this paper presents a discrete-mode load frequency control scheme considering a large sampling period of control/measurement signals via sampled-data control, and introduces an exponential decay rate as a new performance index to guide a design of load frequency control scheme with desired faster frequency response. The proposed scheme is evaluated on a one-area power system, a traditional two-area power system with wind power and a deregulated three-area power system with wind power. Using the proposed scheme and the state-of-the-art schemes, the frequency response performance and the tolerance to sampling period of power systems are analyzed. The results demonstrate that the proposed control scheme can ensure the stable operation of the system under a larger sampling period so as to reduce the communication network burden. Also, the results show that the controller designed by a large exponential decay rate can provide a fast frequency response to alleviate the impact of the system's frequency response due to the high penetration of wind power.

Keywords: Discrete load frequency control, Sampled-data control, Exponential decay rate, Wind power

1. Introduction

Load frequency control (LFC) is designed to restore the balance between load and generation in each control area for maintaining the system frequency and tie-line power between control areas [1]. Measurements of the tie-line power and the frequency are sampled and transferred to the system control centre over communication channels [2]. Plus, a discrete controller is usually implemented on embedded computers in communication channels. Such systems have continuous-time processes and discrete controllers, i.e., the LFC controller is implemented in the discrete-time domain while the power system plant is in the continuous-time domain. Moreover, there is a typical update period (sampling period) of 1–3s for the measurements of the tie-line power and the frequency in practical power system [3]. Therefore, a discrete controller design is required for the LFC as it can take the sampling characteristic into account at the design stage and assure performance in the presence of a large sampling period.

On the other hand, renewable energy sources (RESs), especially wind power [4], have been widely utilized and developed in the last two decades [5]. High penetration of RESs has introduced many new challenges on the operation of modern power system, such as stability issues, uncertainty and low inertia [6, 7]. A reduced inertia of the whole power systems leads to a faster frequency response and larger frequency deviations following a load-generation imbalance [8]. One of the effective solutions is providing faster-acting response against frequency changes. For example, in July 2016, National Grid Electricity System Operator launched and tendered a sub-second frequency response service called Enhanced Frequency Response to improve the whole frequency response structure of UK power market by accelerating the frequency response [9]. Moreover, to accomplish the high penetration of intermittent renewable generations and the increased interaction with the demand-side response, an effective future electricity market tends to employ an open communication infrastructure to support the increasingly decentralized property of control services [10]. Yet the usage of open communication channel with limited network bandwidth introduces unavoidable communication constraints into the LFC scheme

☆This work is supported by the National Natural Science Foundation of China under Grant 61873347, 61503351, and 61573325, the Hubei Provincial Natural Science Foundation of China under Grant 2015CFA010, and the 111 project under Grant B17040.

*Corresponding author
Email address: ljiang@liverpool.ac.uk (Lin Jiang)

[11], including packet dropout and disorder. In order to alleviate those constraints and thus to reduce the communication burden, a larger sampling period is preferred in the power system communication network to reduce the amount of transmitted information and to effectively save the communication bandwidth [12]. Therefore, to improve the performance of LFC for power system with wind power under open communication network, a discrete and fast LFC scheme will show great potential.

Many researchers have made intensive efforts on designing LFC scheme for power systems. Up to date, there are two main methods to accomplish the discrete LFC scheme for power systems. The one is that the controllers are designed in continuous-time mode, and then are discretized and implemented on embedded computers in communication channels. For example, Wang et al. proposed a robust controller in continuous-time mode for power system LFC, based on classical control methods, including the Riccati-equation approach in [13], the H_∞ control approach in [14], the μ–Synthesis method in [15], and the pole assignment method in [16]. Similarly, a robust LFC was proposed for power disturbance and dynamical perturbation of an islanded micro-grid [17]. As an improvement, Tan et al. [18] considered the unmodeled dynamics of power systems to design a robust LFC. As for PID-type controllers, Shayeghi et al. proposed a multi-stage PID to solve the LFC of a deregulated power system [19], and Tan et al. introduced an unified PID tuning method for LFC based on the two-degree-of-freedom internal model control design method [20]. Considering the phenomena of data packet dropout and/or disordering in communication channels, Jiang et al. treated these phenomena as time-varying and random delays, and then investigated the delay-dependent stability [21, 22] and the robust PID-type controller design [23] for the LFC scheme based on Lyapunov theory. Further work can be found in [24]. Considering the penetration of wind power, LFC scheme based on doubly fed induction generator was addressed based on the linear active disturbance approach in [25]. Bevrani et al. addressed a decentralized fuzzy logic-based LFC scheme for interconnected power systems in the presence of high-penetration wind power [26]. However, the above LFC schemes designed in continuous-time mode are only valid in smaller discrete period or sampling period. With the sampling period increasing, the performance of LFC will be degraded or even unstable via discretizing continuous-time controller. Especially, there is a typical update period of 1–3s in practical power system [3].

Another method is based on discretization theory. In [27], a method of designing discrete–type load–frequency regulators of a two-area reheat–type thermal system with generation-rate constraints was presented. Thereafter, Vrdoljak et al. introduced a discrete-time LFC scheme in [28], using sliding mode control (SMC) with fast output sampling technique. As an improvement, an event-triggered SMC scheme for the LFC problem in multi-area power systems was proposed in [29], and a decentralised LFC strategy was introduced for multi-area time-delay power system with significant wind power penetration in [30]. Furthermore, Cui et al. investigated the LFC for wind power systems with modeling uncertainties and variant loads based on observer-based robust integral SMC in [31]. Zhang et al. solved the design problem of digital PID-type controller based on discrete-time LFC model for power system with time delays in [32]. A coordinated distributed model predictive control for the LFC of a power system considering inherently variable wind-power generations was presented in [33]. Yet they were designed based on the directly discretized plant model with regarding sampling period as discretized period. Note that the control signal is updated every 1–3s in hydrothermal power system [3]. When the discretized period is set to 1–3s against the time constants lying in the range 0.08–0.3s in hydrothermal power system, it cannot follow the Shannon sampling principle [2]. Fridman introduced an input delay method to analyze such continuous-discrete sampled-data system in [34], which avoids effectively the problem of discrete distortion. Based on this method, discrete sampled-data controllers were designed in a simple one-area power system in [35] and an isolated hybrid power system in [12]. To reduce communication burden and save communication bandwidth, Wen et al. designed a sampled-data based event-triggered LFC scheme with continuous-time PI or PID controllers in [36]. As an improvement, Dong et al. presented a event-triggered LFC scheme with supplementary adaptive dynamic programming in [37], and an adaptive event-triggered LFC scheme was introduced in [38]. However, the considered sampling periods are all less than 1s, which does not match practical update period of control/measurement signals.

As for the fast LFC scheme for power systems, battery energy storage systems were applied due to their fast response to load-generation imbalance in [39]. Electric vehicles as an application of controllable loads are used to fast regulate frequency deviation of power systems in the presence of intermit injection of RESs in [40]. As an improvement, considering compensation of communication latency and detection error in frequency regulation process, a hybrid modeling and control of controllable loads for LFC was proposed in [41]. Also, a virtual inertia controller provided by DFIG-wind turbines was designed to faster suppress frequency fluctuations in [42, 43]. Jia et al. presented a coordinated control strategy between electric vehicles-LFC controller and traditional power plants based LFC controller for primary frequency regulation in [44]. Note that all the above LFC schemes focus on the primary frequency regulation. Although these control strategies can fast generate effectively actions to restore the balance, a new secondary frequency controller design method needs to be proposed to conform with desired faster frequency regulation requirement in combination with above hybrid (continuous-discrete) power systems.

Motivated by above discussions, this paper proposes a discrete and fast LFC scheme for power system with wind

power under open communication network. The originality and contributions of this paper can be summarized as follows:

1) A discrete-mode LFC scheme is designed directly based on sampled-data control scheme. The previous studies mainly pay attention to designing continuous controller and do not consider the impact of a large sampling period. In comparison with continuous-mode controller in [19] and [20], the proposed discrete LFC scheme can be directly used in power system without the performance degradation caused by discretization and the instability resulting from a larger discrete period.
2) It is different from the directly discretized design method in [27], the input delay method is employed to transform sampled-data LFC system into time delay system and circumvents effectively discrete problem disobeying Shannon sampling theorem. Such method takes fully the sampling characteristic into account. The proposed LFC scheme can assure the stable operation of power systems over a large sampling period of control/measurement signals in open communication network so as to save network resources and to reduce communication burden.
3) To deal with the faster frequency response and bigger frequency deviation resulting from the reduced inertia of power system, EDR is introduced to guide the design of a discrete LFC with desired faster frequency regulation requirement. The proposed fast LFC scheme focuses on the secondary frequency controller to shorten duration of the total frequency regulation, compared with using the primary frequency regulation in previous studies.
4) A design procedure for LFC scheme, which integrates sampling period and EDR, is presented. By adjusting the parameters of sampling period and EDR, different requirements of LFC design can be realized, including reducing the communication network burden and faster frequency response speed.

The remainder of this paper is organized as follows. Section 2 gives the dynamic model of the discrete LFC scheme based on sampled-data control. Section 3 proposes a method of controller design of the discrete and fast LFC scheme. In Section 4, case studies based on traditional one-area LFC, traditional two-area and deregulated three-area LFC with wind power are shown to verify effectiveness of the proposed method. Conclusion is given in Section 5.

2. Dynamic model of discrete LFC scheme

This section describes a discrete model of traditional and deregulated LFC scheme with wind power. As shown in Fig. 1, the structure of control area i includes n traditional generation units, wind power, tie-line power and communication network. In the traditional LFC scheme, the generation unit represents an unit of generators, while it represents a generation company (Genco) in the deregulated LFC scheme. For simplicity, the time delay existing in signal transmission can be negligible when the update periods of measurement signals and control signals between 1–3s. Also, it is assumed that all traditional generators are equipped with non-reheat turbine. The model of the wind power is reduced as following equation (2).

2.1. Continuous-time Model of power system plant

Excluding the dotted line connection of Fig. 1, the LFC model of i area of a traditional multi-area power system including N control areas and n units of generators can be derived from [3]

$$\dot{\bar{x}}_i(t) = \bar{A}_i\bar{x}_i(t) + \bar{B}_i u_i(t) + \bar{F}_i\bar{\omega}_i(t) \tag{1}$$

where

$\bar{x}_i^T = [\Delta f_i\ \Delta P_{tie-i}\Delta P_{m1i}\cdots\Delta P_{mni}\ \Delta P_{v1i}\cdots\Delta P_{vni}]$

$u_i = \Delta P_{Ci}, \bar{\omega}_i = [v_{1i}\ v_{2i}]^T = [\Delta P_{di}\ \sum_{j=1,j\neq i}^{N} T_{ij}\Delta f_j]^T$

$$\bar{A}_i = \begin{bmatrix} A_{11i} & A_{12i} & 0 \\ 0 & A_{22i} & A_{23i} \\ A_{31i} & 0 & A_{33i} \end{bmatrix} \bar{B}_i = \begin{bmatrix} 0 \\ 0 \\ B_{3i} \end{bmatrix} \bar{F}_i = \begin{bmatrix} -\frac{1}{M_i} & 0 \\ 0 & -2\pi \\ 0 & 0 \end{bmatrix}$$

$$A_{11i} = \begin{bmatrix} -\frac{D_i}{M_i} & -\frac{1}{M_i} \\ 2\pi\sum_{j=1,j\neq i}^{N} T_{ij} & 0 \end{bmatrix} A_{12i} = \begin{bmatrix} \frac{1}{M_i} & \cdots & \frac{1}{M_i} \\ 0 & \cdots & 0 \end{bmatrix}$$

$$A_{22i} = -A_{23i} = diag\left\{\frac{-1}{T_{ch1i}}\cdots\frac{-1}{T_{chni}}\right\} B_{3i} = \begin{bmatrix} \frac{\alpha_{1i}}{T_{g1i}}\cdots\frac{\alpha_{ni}}{T_{gni}} \end{bmatrix}$$

$$A_{31i} = \begin{bmatrix} \frac{-1}{RT_{g1i}} & \cdots & \frac{-1}{RT_{gni}} \\ 0 & \cdots & 0 \end{bmatrix}^T A_{33i} = diag\left\{\frac{-1}{T_{g1i}}\ \cdots\ \frac{-1}{T_{gni}}\right\}.$$

and $\Delta f_i, \Delta P_{mki}, \Delta P_{vki}$, ΔP_{Ci} and ΔP_{di} are the deviation of frequency, generator mechanical output, valve position, control input and the disturbance of load demand, respectively; $M_i, D_i, T_{gki}, T_{chki}, R_{ni}$ and α_{ki} represent the moment of inertia of generator unit, generator unit damping coefficient, time constant of the governor, time constant of the turbine, speed droop and the ramp rate factor, respectively; ΔP_{tie-i} represents the tie-line power exchange and T_{ij} is the tie-line synchronizing coefficient between the i_{th} and j_{th} control area; $\bar{\omega}_i$ represents the disturbances of the system, including v_{1i} the disturbance of load demand and v_{2i} the interactions between area i and the other areas.

The area control error (ACE) signal in such scheme is defined as $ACE_i = \beta_i\Delta f_i + \Delta P_{tie-i}$ where β_i is frequency bias factor. In order to force the steady state of Δf_i and ΔP_{tie-i}, the integral of ACE is used as an additional state variable, it is defined as $\Delta E_i = K_{I_i}\int ACE_i(t)d(t)$ where K_I is the gain of integral part. When wind power is introduced into power system, the low-order dynamical model of wind turbine generator (WTG) is considered as follow [17]:

$$\Delta P_{WTGi}(s) = \frac{1}{1+sT_{WTGi}}\Delta P_{w-i}(s) \tag{2}$$

where ΔP_{WTGi} and ΔP_{w-i} represent the output power

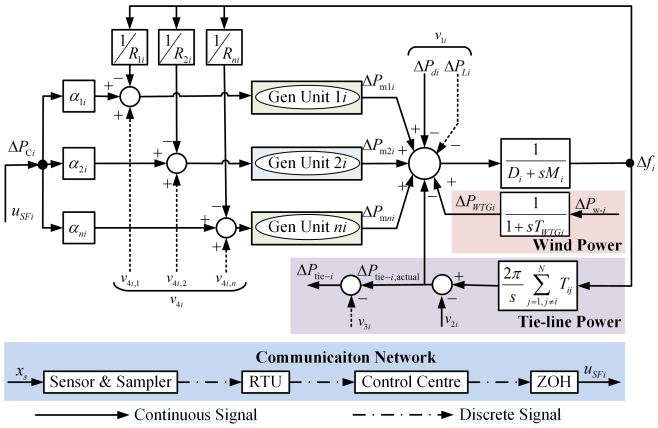

Figure 1: Dynamical model of the ith control area of LFC scheme for a multi-area power systems with wind power.

change of WTG and wind power in area i, respectively; and T_{WTGi} is the time constant of WTG in area i. Then, the state variables of ΔE_i and ΔP_{WTGi} are added into model (1), the state space model can be constructed as

$$\dot{x_i}(t) = A_i x_i(t) + B_i u_i(t) + F_i \omega_i(t) \tag{3}$$

where

$$x_i{}^T = [\bar{x}_i^T \ \Delta E_i \ \Delta P_{WTGi}] \ w_i = [\bar{w}_i; \ \Delta P_{w-i}]$$

$$A_i = \begin{bmatrix} \hat{A}_{11i} & \hat{A}_{12i} \\ 0 & \frac{-1}{T_{WTGi}} \end{bmatrix} \hat{A}_{11i} = \begin{bmatrix} \bar{A}_i, 0 \\ K_{Ii}\beta_i, K_{Ii}, 0 \end{bmatrix}$$

$$\hat{A}_{12i} = \begin{bmatrix} \frac{1}{M_i} \\ 0 \end{bmatrix} B_i = \begin{bmatrix} \bar{B}_i \\ 0 \end{bmatrix} F_i = diag\left\{\hat{F}_i, \frac{1}{T_{WTGi}}\right\} \hat{F}_i = \begin{bmatrix} \bar{F}_i \\ 0 \end{bmatrix}.$$

For multi-area LFC in deregulated environment including N control areas, each control area i consists of m distribution companies (Discos) and n Gencos, as shown in Fig. 1 with the dotted line connection. The state-space model of control area i of deregulated LFC scheme is same as model (3) excluding [23]

$$\hat{F}_i = \begin{bmatrix} \tilde{F}_i \\ 0 \end{bmatrix}, \tilde{F}_i = \begin{bmatrix} F_{i11} & 0 \\ 0 & 0 \\ 0 & F_{i32} \end{bmatrix}, F_{i11} = \begin{bmatrix} \frac{-1}{M_i} & 0 & 0 \\ 0 & -2\pi & 0 \end{bmatrix}$$

$$F_{i32} = diag\left\{\frac{1}{T_{g1i}} \cdots \frac{1}{T_{gni}}\right\}, w_i^T = [v_{1i}^T \ v_{2i}^T \ v_{3i}^T \ v_{4i}^T]$$

and v_{3i} and v_{4i} are given in [23] and are omitted due to limited space. It is noteworthy that when considering a stand-alone power system, power exchange in the tie-line between control areas does not exist and ΔP_{tie-i} vanishes in model (3).

2.2. Discrete LFC model via input delay method

In continuous-time mode, the state variables x_s are directly used for the generation of the control signal. However, in discrete-time mode, only discrete measurements of x_s can be used for LFC scheme based on sampled-data control, that is, only the measurements $x_i(t_k)$ at sampling instant t_k are considered. As shown in Fig. 1, the state variables x_s are quantized and sampled by sensors and samplers at sampling instant t_k, and then the sampling information is transmitted from the RTU to the control center, where the control signals will be processed via discrete controller. Finally, the control signal u_{SF} is transmitted to the continuous-time plant by ZOH. It is assumed that the sampling instants t_k $(k = 0, \ 1, \ 2, \cdots)$ satisfy

$$0 = t_0 < t_1 < \cdots < t_k < \cdots < \lim_{k\to\infty} t_k = +\infty \tag{4}$$

$$\Delta k = t_{k+1} - t_k = h_k \leq h_M \tag{5}$$

where h_M represents maximum sampling period. Based on the input delay method [34], the discrete controller is designed at sampling instant t_k as follow

$$\begin{cases} u_{SFi}(t_k) = K_{SFi} x_i(t_k) \\ u_i(t) = u_{SFi}(t_k) \end{cases} \qquad t_k \leq t < t_{k+1} \tag{6}$$

where K_{SFi} is the gains of discrete controller. Combining (3) and (6), the dynamic model of sampled-data LFC can be derived as follow

$$\dot{x_i}(t) = A_i x_i(t) + B_i K_{SFi} x_i(t_k) + F_i \omega_i(t) \tag{7}$$

where $t_k \leq t < t_{k+1}, \ k = 0, \ 1, \ 2, \cdots$.

Remark 1. Based on input delay method, the continuous-discrete LFC model is transformed into piecewise continuous model in every sampling interval $[t_k, t_{k+1})$. Then, with the aid of the theory of piecewise continuous system [45, 46], the theorems of stability analysis and controller design are derived in the section III. In this way, unlike the directly discretized design method used in the literature [27, 29, 32] to analyze the system stability and design the controller, the problem of discrete distortion is effectively avoided.

In above model, the interactions between different areas are treated as disturbances, i.e., v_{2i}. Thus, the design of multi-area discrete load frequency controller K_{SFi} is simplified to a repetitive single-area design problem. Also, the balance point's inner stability of the system (7) is equivalent to the origin's stability with $\omega(t) = 0$. Thus, the state-space model studied in this paper can be summarized as follows

$$\dot{x}(t) = Ax(t) + BK_{SF}x(t_k) \tag{8}$$

where $t_k \leq t < t_{k+1}, \ k = 0, 1, 2, \cdots$.

3. Design of discrete LFC scheme

In this section, the design of the discrete LFC scheme for one-area power system is introduced. EDR is introduced as a performance index to guide the design of controller. Then, two theorems of stability and controller design are proposed based on EDR. For multi-area power system, the discrete LFC scheme for each control area can still be designed as that in a one-area system, in which only local system information is needed to design such controller.

In order to design the controller, EDR and the stability are firstly introduced as the following subsection.

3.1. The introduction of EDR and stability criterion

Systems are exponentially stable if their convergence is bounded by EDR. EDR reflects the dynamical performance of system. The margin of EDR depends on the selection of controller. For a given controller, the following theorem is proposed to verify the exponential stability of one-area power system and to calculate the margin of EDR.

Theorem 1. *Consider system (8), for given EDR λ, sampling period h and designed controller K_{SF} if there exist symmetric matrices $X_i = \begin{bmatrix} X_{1i}+X_{1i}^T & -X_{1i}-X_{2i} \\ * & X_{2i}+X_{2i}^T \end{bmatrix}$, R_{1i}, R_{2i}, V_i, and R_{3i}, and symmetric positive definite matrices P_i, R_{3i}, and any appropriately dimensioned matrices N_{1i}, N_{2i}, L_i, M such that the following conditions hold:*

$$\Psi_{1i} = \Xi_{1i} + h\Xi_{2i} < 0 \tag{9}$$

$$\Psi_{2i} = \begin{bmatrix} \Xi_{1i} - he_2^T R_{2i} e_2 & -h\Upsilon L_i \\ * & -hR_{1i} \end{bmatrix} < 0 \tag{10}$$

where $i = 1, 2$ and the detailed elements of the matrices Ψ_{1i} and Ψ_{2i} are shown in Appendix. Then, system (8) is exponentially stable and has a dynamic performance index λ.

Proof. Choose following Lyapunov–Krasovskii functional

$$V(x_t) = V_1(x_t) + V_2(x_t) \tag{11}$$

where

$$V_1(x_t) = x^T(t)Px(t)$$

$$V_2(x_t) = h_{\tau(t)}({\xi_1}^T \begin{bmatrix} X & N_1 \\ * & V \end{bmatrix} \xi_1 + \int_{t_k}^{t} {\xi_2}^T \begin{bmatrix} R_2 & N_2 \\ * & R_3 \end{bmatrix} \xi_2 ds)$$

and $h_{\tau(t)} = h - \tau(t)$, $\xi_1 = [x^T(t), x^T(t_k), \int_{t_k}^{t} x^T(s)ds]^T$, $\tau(t) = t - t_k$, $\xi_2 = [x^T(t_k), x^T(s), \dot{x}^T(s)]^T$. Define $\zeta_1(t) = [x^T(t), x^T(t_k), \dot{x}^T(t)]^T$ and $\zeta(t) = [{\zeta_1}^T(t), \int_{t_k}^{t} x^T(s)ds]^T$. Based on Newton-Leibnitz formula,

$$0 = 2\zeta^T(t)L\left(x(t) - x(t_k) - \int_{t_k}^{t} \dot{x}(s)ds\right) \tag{12}$$

$$0 = 2\zeta_1^T(t)M\left(\dot{x}(t) - Ax(t) - BK_{SF}x(t_k)\right) \tag{13}$$

Then, calculating the time derivation of $V(x_t)$ along $t \in (t_k, t_{k+1})$, using Jensen inequality to estimate integral item of R_3 and adding equations (12) and (13), the derivative of $V(x_t)$ satisfies

$$\dot{V}(x_t) = \frac{h_{\tau(t)}}{h}\zeta^T(t)\Psi_1\zeta(t) + \frac{1}{h}\int_{t_k}^{t} \begin{bmatrix} \zeta(t) \\ \dot{x}(s) \end{bmatrix}^T \Psi_2 \begin{bmatrix} \zeta(t) \\ \dot{x}(s) \end{bmatrix} ds$$

where Ψ_1 and Ψ_2 are defined in Theorem 1 without the subscript i and $\Gamma = Sym\left(\Pi^T M(e_3 - Ae_1 - BK_{SF}e_2)\right)$.

Note that for $k = 0, 1, 2\cdots$, $V_2(x_{t_k}) = V_2(x_{t_{k+1}})$ and if $\Psi_1 < 0$ and $\Psi_2 < 0$ hold, $\dot{V}(x_t) < 0$. So, system (8) is asymptotically stable according to theorem 1 in [45]. Then, based on remark 5 in [46], if (9) and (10) hold, system (8) is exponentially stable. This completes the proof.

For a designed discrete controller K_{SF}, and given sampling period h, the exponential stability of system can be verified by developing the feasibility of linear matrix inequations (LMIs) (9) and (10) by maximizing EDR λ_M. The margin of EDR can be determined by λ_M.

Secondly, the controller design criterion is introduced based on the above stability condition. When controller is unknown, Theorem 1 is no longer LMI-based condition due to a product of M_iBK_{SF}. To solve this problem, the following subsection is shown to derive the controller parameters.

3.2. Controller design criterion

Theorem 2. *Consider system (8), for given EDR λ and sampling period h, if there exist symmetric matrices $\hat{R}_{1i}$, $\hat{R}_{2i}$, $\hat{V}_i$, $\hat{R}_{3i}$ and $\hat{X}_i$, and symmetric positive definite matrices $\hat{P}_i$, $\hat{R}_{3i}$, and any appropriately dimensioned matrices $\hat{N}_{1i}$, $\hat{N}_{2i}$, $\hat{L}_i$, $M = [S; aS; bS]$, $\hat{S} = S^{-1}$, $Y = K_{SF}\hat{S}^T$ and tuning parameters a and b such that the following conditions hold:*

$$\hat{\Psi}_{1i} = \hat{\Xi}_{1i} + h\hat{\Xi}_{2i} < 0 \tag{14}$$

$$\hat{\Psi}_{2i} = \begin{bmatrix} \hat{\Xi}_{1i} - he_2^T \hat{R}_{2i} e_2 & -h\Upsilon\hat{L}_i \\ * & -h\hat{R}_{1i} \end{bmatrix} < 0 \tag{15}$$

where $i = 1, 2$, $\Gamma_i = Sym(\Pi^T\Pi_5(\hat{S}^T e_3 - (A + \lambda I)\hat{S}^T e_1 - \rho_i BY e_5))$, $\Pi_5 = [I; aI; bI]$ and the other parameters are given in Theorem 1 with superscript $\hat{}$. Then system (8) is exponentially stable under the effect of controller

$$K_{SF} = Y(\hat{S}^T)^{-1}. \tag{16}$$

Proof. Define $\hat{P}_i = \hat{S}P_i\hat{S}^T$, $\hat{R}_1 = \hat{S}R_1\hat{S}^T$, $\hat{R}_2 = \hat{S}R_2\hat{S}^T$, $\hat{L}_i = diag\{\hat{S}, \hat{S}, \hat{S}, \hat{S}\}L_i\hat{S}^T$, $\hat{N}_{1i} = diag\{\hat{S}, \hat{S}\}N_{1i}\hat{S}^T$, $\hat{V}_i = \hat{S}V_i\hat{S}^T$, $\hat{N}_{2i} = \hat{S}N_{2i}diag\{\hat{S}^T, \hat{S}^T\}$, $\hat{X}_i = diag\{\hat{S}, \hat{S}\}X_i diag\{\hat{S}^T, \hat{S}^T\}$, pre and post multiply (9) by $diag\{\hat{S}, \hat{S}, \hat{S}, \hat{S}\}$ and its transpose, respectively, and pre and post multiply (10) by $diag\{\hat{S}, \hat{S}, \hat{S}, \hat{S}, \hat{S}\}$ and its transpose, respectively. Then, (14) and (15) are obtained. This completes the proof.

Inequalities (14) and (15) are determined by giving appropriate λ and h, and thus the values of matrices Y and $\hat{S}$ are obtained. Then, the controller parameters are calculated through equation (16). To meet different requirements, such as fast frequency response speed or reducing communication network burden, the proposed method can achieve the controller design with different performance. The detailed procedure is introduced in the following subsection.

3.3. Procedure of discrete LFC scheme design

The detailed procedure of the proposed method is summarized as the following steps.

S1 Model derivation and determine the system parameters.

S2 Controller design. If sampling period h_g is given, go to S2.1; if EDR λ_g is given, go to S2.2; if they are both given, go to S2.3.

S2.1 1) Initialize the search interval $[\lambda_{min}, \lambda_{max}]$ with $\lambda_{min} = 0$ and large enough number λ_{max} and select the accuracy coefficient $\lambda_{ac} = 0.001$. 2) Determine whether the system has a test EDR given as $\lambda_{test} = (\lambda_{min} + \lambda_{max})/2$ by checking the feasibility of LMIs (14) and (15). 3) If (14) and (15) are feasible, set $\lambda_{min} = \lambda_{test}$; else, set $\lambda_{max} = \lambda_{test}$. 4) If $|\lambda_{min} - \lambda_{max}| \leq \lambda_{ac}$, obtain the maximum EDR $\lambda_M = \lambda_{min}$ and derive gains of controller by calculating (16); else, repeat 2).

S2.2 Initialize the search interval $[h_{min}, h_{max}]$ with $h_{min} = 0$ and large enough number h_{max} and select the accuracy coefficient $h_{ac} = 0.1$. Then, use the same steps in S2.1 to obtain gains of controller and the maximum sampling period h_M.

S2.3 1) Fix sampling period h_g and go to S2.1, then obtain maximum EDR λ_M. 2) Compare λ_M with the given EDR λ_g. If $\lambda_M \geq \lambda_g$, the feasibility of LMIs (14) and (15) is assured. Then bring directly h_g and λ_g into Theorem 2 and derive gains of controller by calculating (16). If $\lambda_M < \lambda_g$, the controller can not be found.

S3 Simulation verification. Simulation studies are carried out to verify the effectiveness of the proposed controller with respect to different disturbances.

In S2.1, the gains of controller with a faster frequency response are determined by maximizing the EDR. Similarly, in S2.2, in order to enable controller to operate stably over a larger sampling period and thus to reduce communication burden, the gains are obtained by maximizing the sampling period. The maximum EDR (MEDR) or the maximum acceptable sampling period (MASP) obtained can also provide guidance for controller design. This is well represented in S2.3. If both requirements are given, the MEDR can be obtained through S2.1. If the requirement of EDR exceeds the maximum, the controller gains cannot be obtained. Then, it is necessary to appropriately lower requirements of sampling period and/or EDR to achieve a trade-off between the two requirements so as to assure the controller design.

Remark 2. Theorem 1 provides a method to evaluate the designed controller. When the controller is given, the MASP that the system can tolerate is obtained by setting a fixed EDR, or the MEDR of the system is obtained by setting a fixed sampling period. If the system has larger MASP or MEDR via a controller, then this controller is considered to have better performance. It is worth noting that the PID controller can also be evaluated by this method, because it can be transformed into a state feedback controller by multiplying the corresponding output matrix. This will be used in subsequent comparisons of different controllers.

Remark 3. Based on Theorem 2, this method has the following two advantages. First, when the EDR is fixed, the controller designed by maximizing sampling period enable the power system to operate stably under a larger sampling period so as to reduce the communication burden. Secondly, when the sampling period is fixed, the controller designed by maximizing EDR can make the power system provide faster frequency response speed in order to deal with the problem of faster frequency fluctuation due to the reduced inertia of the power system.

4. Case studies

In this section, effectiveness of the proposed discrete LFC scheme is demonstrated based on one-area power system, traditional two-area and deregulated three-area power system with wind power. A one-area power system is considered to illustrate the necessity of designing controllers in discrete-time mode instead of continuous-time mode. Also, a traditional two-area power system with wind power is introduced to show the influence on frequency fluctuation of the system due to the high penetration of wind power and to illustrate that the proposed controller can provide a faster frequency response speed. Lastly, a deregulated three-area power system with wind power is considered to further demonstrate the effectiveness of the proposed method, including the two advantages shown in the above two cases.

4.1. One-area LFC

The detailed model of one-area LFC scheme is shown in Fig. 2, and the parameters are listed in Table 6 in appendix [18]. Assume that the sampling period is set to 2s.

4.1.1. Controller design

By setting $a = 0$, $b = 2.03$, $\lambda_{min} = 0$, and $\lambda_{max} = 3$, and following the procedure described in S2.1, gains of discrete controller (named as K_1) are obtained and the MEDR is $\lambda_M = 0.39$. The parameters of K_1 obtained is shown in Table 1.

4.1.2. Comparison and analysis

To illustrate the difference between the controller designed in discrete-time mode and continuous-time mode, five different continuous-time controllers are given. Based on continuous-time mode, the continuous-time controllers $K_2 - K_6$ were derived in [13, 14, 15, 16, 20], respectively. Controllers $K_2 - K_5$ are all the state-feedback type as the same as this paper, while controller K_6 is the PID

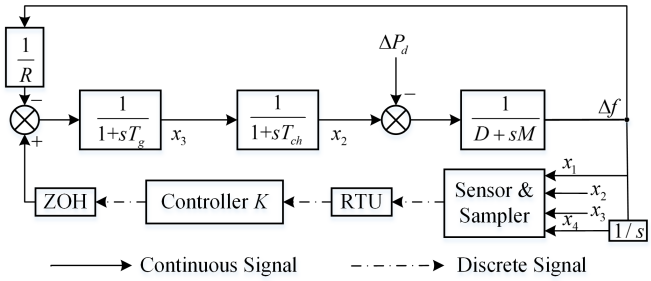

Figure 2: Detailed LFC model of one-area power systems.

Table 1: Parameters and MASPs of different load frequency controllers of one-area power system

Controllers	Parameters	MASPs(s)
K_1[this paper]	-[0.0622 0.1231 0.0226 0.1723]	4.50
K_2[13]	-[1.893 4.762 1.516 1.658]	0.11
K_3[14]	-[5.03 8.7258 2.1324 1.6252]	0.07
K_4[15]	-[2.7321 4.0167 0.8506 0.4318]	0.19
K_5[16]	-[13.738 16.077 2.837 19.118]	0.05
K_6[20]	-[0.4036 0.6356 0.1832]	0.62

type. The parameters of $K_2 - K_6$ are also shown in Table 1. When the one-area power system is equipped with $K_1 - K_6$, mathematical analysis and simulation test are carried out.

For every controller, MASPs of the system are calculated via Theorem 1 with $\lambda = 0$. The results are listed in the Table 1. From these results, it can be found that $K_2 - K_6$ can maintain the stability of the system under a smaller sampling period (less than 0.62s), while the controller obtained in this paper can reach at 4.50s. Then, the system is tested in the presence of step change $\Delta P_d = 0.01\ pu$ (for $t \geq 0$) of load demand. Responses of frequency deviation are shown in the Fig. 3 under different sampling periods. From Fig. 3 (a), when $h = 0.05s$, K_2, K_5 and K_6 spend less time driving the frequency deviation back to zero than K_1, K_3 and K_4. However, with increase of sampling period, $K_2 - K_5$ cannot generate effective action to maintain the stability of system when $h \geq 0.5s$ as shown in Fig. 3 (b). Especially, the continuous-time controllers K_2-K_6 all result in instability when $h \geq 1s$ from Fig. 3 (c) and (d), while K_1 designed in this paper can still remain stability. These results are consistent with the mathematical analysis. It demonstrates that the discrete-mode controller designed in this paper can be directly used in power system without the performance degradation caused by discretization. Moreover, the results also show that the proposed scheme can assure the usage of a larger discrete period so as to reduce communication network burden. Yet the continuous-time controller will degrade system performance and even cause system instability under a larger sampling period. Therefore, the design of the discrete controller is necessary for the real power system under open communication network.

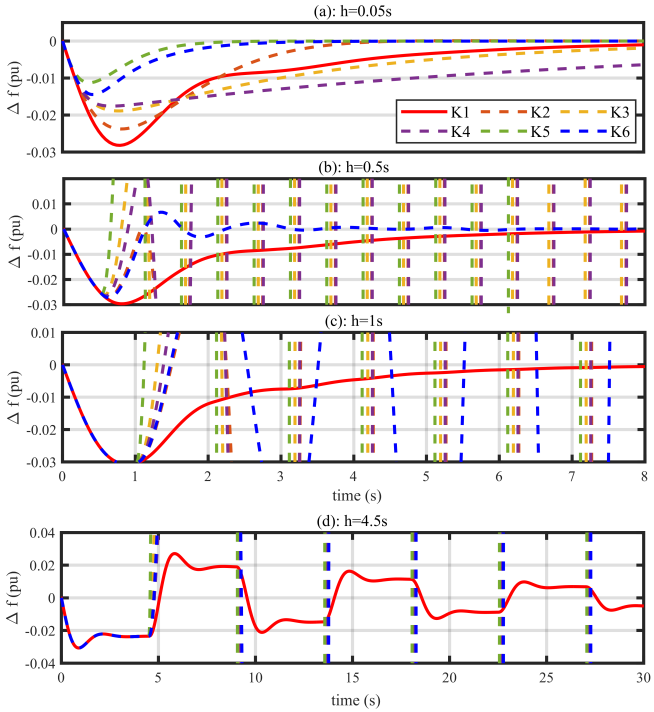

Figure 3: Frequency responses of one-area LFC scheme equipped with load frequency controllers $K_1 - K_6$ under sampling periods h=0.05s, 0.5s, 1s and 4.5s.

4.2. Traditional two-area LFC with wind power

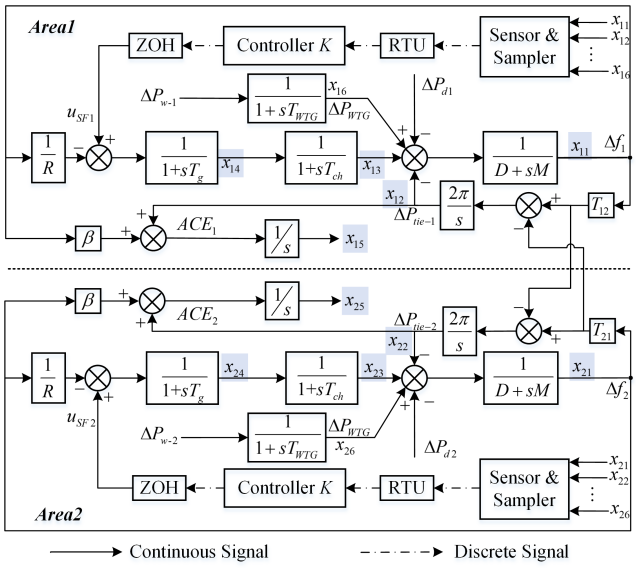

Figure 4: Detailed LFC model of traditional two-area power systems with wind power.

The detailed model of traditional two-area LFC with wind power is shown in Fig. 4, where each area of the traditional two-area power system includes one generation unit and transmission delays of control signal are all considered as 0.2s in two areas. As reported in [8], inertia constant M, speed droop constant R and frequency bias factor β of the system will be modified with the increase of penetration of wind power, and wind penetration level will be illustrated with different values of inertia reduction

(IR). Assume that parameters of two areas with 40% IR are set to be same and are reported in Table 7 in Appendix.

4.2.1. Controller design

Discrete controllers $K_7 - K_{10}$ are deigned following two different requirements, and their parameters are reported in Table 2.

Controller Design 1 [Given sampling period based on requirement of communication network]: Sampling periods are set to $h_{g1} = 1s$ and $h_{g2} = 5s$, respectively. Controllers K_7 and K_8 are derived by setting $a = 0$, $b = 2.03$, $\lambda_{min} = 0$, and $\lambda_{max} = 3$ and following the algorithm in S2.1, in which maximum EDRs $\lambda_{M1} = 0.19$ and $\lambda_{M2} = 0.13$ are obtained.

Controller Design 2 [Given EDR based on requirement of frequency response speed]: EDRs are set to $\lambda_{g1} = 0.05$ and $\lambda_{g2} = 0.25$, respectively. By setting $a = 0$, $b = 2.03$, $h_{min} = 0$, and $h_{max} = 15$ and following the algorithm in S2.2, controllers K_9 and K_{10} are developed and maximum sampling periods $h_{M1} = 9.6s$ and $h_{M2} = 0.5s$ are obtained.

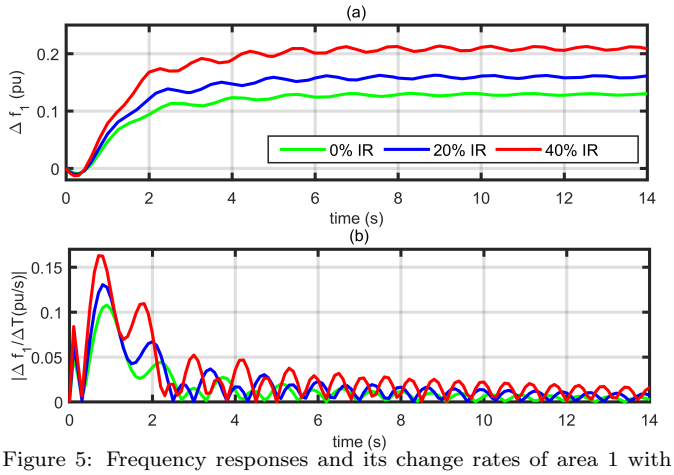

Figure 5: Frequency responses and its change rates of area 1 with different levels of wind power penetration under only primary control.

4.2.2. Comparison and analysis

Firstly, to illustrate changes of frequency response due to reduced inertia, the system is tested in different wind penetration levels and is only controlled by primary control loop. Frequency responses of area 1 are shown in Fig. 5(a) when subjected to step disturbances $\Delta P_{d1} = 0.01pu$ and $\Delta P_{d2} = 0.02pu$ (for $t \geq 0$) and step changes $\Delta P_{wind1} = 0.04pu$ and $\Delta P_{wind2} = 0.06pu$ of wind power deviation (for $t \geq 0$). Define the rate of change of frequency (RoCoF) by $|\Delta f/\Delta T|$. By setting $\Delta T = 0.1s$, the RoCoF of area 1 is shown in Fig. 5(b). As can be seen from Fig. 5, frequency responses of the system show a faster frequency changes and larger frequency deviation with the higher penetration of wind power, when the system is only controlled.

Secondly, in order to illustrate that the proposed LFC scheme can make the system provide faster frequency response to cope with the problem of faster frequency changes and larger frequency deviation as described above, the following two comparisons and analysis are carried out.

*Comparison 1 [Comparison of the designed controllers in this paper]:*The system equipped with K_7-K_{10} operates over sampling periods of $h_{g1} = 1s$, $h_{g2} = 5s$, $h_{M1} = 9.6s$ and $h_{M2} = 0.5s$, respectively. Also, the system equipped with every controller is tested in different wind penetration levels. Assume that the system is subjected to step change $\Delta P_{d2} = 0.04pu$ of load demand (for $t \geq 0$) and step changes $\Delta P_{wind1} = 0.04pu$ and $\Delta P_{wind2} = 0.06pu$ of wind power deviation (for $t \geq 0$). Frequency responses of area 1 controlled by K_7-K_{10} are shown in Figs. 6-9, respectively.

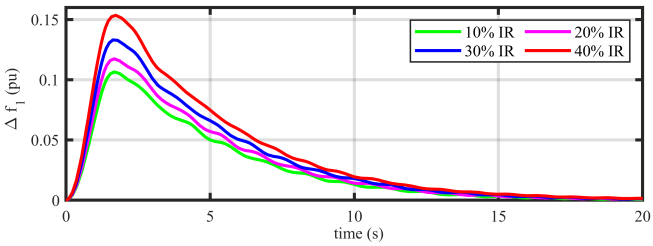

Figure 6: Frequency responses of area 1 with different levels of wind power penetration under sampling period $h = 1s$ and EDR $\lambda = 0.19$.

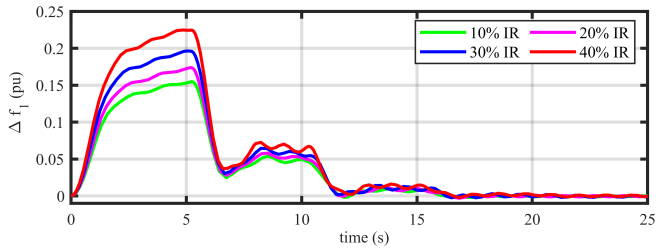

Figure 7: Frequency responses of area 1 with different levels of wind power penetration under sampling period $h = 5s$ and EDR $\lambda = 0.13$.

From Figs. 6-9, the system controlled by controllers $K_7 - K_{10}$ can restore the balance between generation and load at 13s, 18s, 45s and 10s, respectively. These results show that the controller designed at a higher penetration of wind power (40% IR) can operate well at lower levels (10%, 20% and 30% IR) and maintain almost same frequency response speed. It can also be seen that K_{10} designed by setting $\lambda = 0.25$ has the fastest frequency response speed performance. In combination with Fig. 5, it can be seen that EDR as the performance factor can guide the design of a discrete LFC with desired frequency response speed. Furthermore, the larger the EDR, the faster the frequency response speed of the LFC scheme. Therefore, the simulation results show that the proposed fast LFC scheme can cope with the problem of faster frequency changes and larger frequency deviation resulting from the reduced inertia due to high penetration of wind power by adjusting a larger EDR.

On the other hand, the mutual constraint between the requirements of communication network and frequency response speed is also shown in the above results. K_{10} only operates stably in the power system within smaller sampling period (0.5s), while K_9 designed by $\lambda_g = 0.05$ ensure that the system restores the balance within a larger sampling period (9.6s). In order to better show their relationship, the MEDRs corresponding to the requirement

Table 2: Load frequency controller parameters for traditional two-area power systems with wind power under different requirements

$h_{g1} = 1s$	K_7=-[0.0194 -0.0036 0.0895 0.0059 0.2246 0.3391]
$h_{g2} = 5s$	K_8=-[0.0130 -0.0013 0.0582 0.0061 0.1444 0.2178]
$\lambda_{g1} = 0.05$	K_9=-[0.0060 0.0000 0.0240 0.0047 0.0599 0.0899]
$\lambda_{g2} = 0.25$	K_{10}=-[-0.0215 -0.1496 0.1360 -0.0176 0.2681 0.5223]

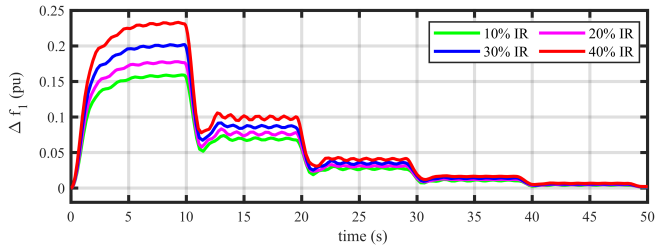

Figure 8: Frequency responses of area 1 for traditional two-area power systems with different levels of wind power penetration under EDR $\lambda = 0.05$ and sampling period $h = 9.6s$.

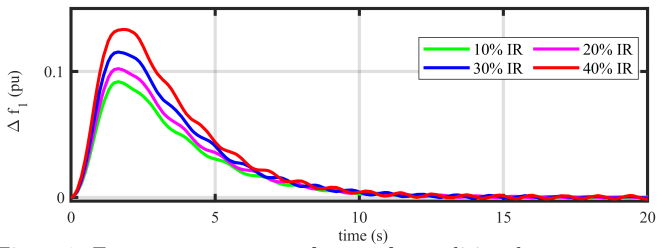

Figure 9: Frequency responses of area 1 for traditional two-area power systems with different levels of wind power penetration under desired EDR $\lambda = 0.25$ and sampling period $h = 0.5s$.

of sampling period are listed in Table 3. With increase of sampling period, the margin of EDR will decrease. Therefore, the proposed LFC design can meet different requirements of reducing the communication network burden or faster frequency response speed by adjusting appropriate sampling period or EDR. Based on the results in Table 3, it also provides a boundary condition to guide the design of the controller. As long as the requirements of sampling period and EDR are not out of the bound of h_g and λ_M, the controller that meets the requirements can be designed.

Table 3: MEDRs of LFC scheme of traditional two-area power system with wind power under differently maximum sampling periods

h(s)	0.5	2	3.5	5	6.5	8	9.5	11	12.5
λ	0.254	0.198	0.198	0.133	0.087	0.065	0.052	0.041	0.029

Comparison 2 [Comparison of the designed controller and discrete PI controllers]: The control effects are compared between the proposed controller K_8 and discrete PI controllers ($K_{PI1} = [0.2, 0.1]$, $K_{PI2} = [0.4713, 0.1162]$). K_{PI1} is adjusted manually, while K_{PI2} is well-tuned by PSO algorithm [47]. In the PSO algorithm, the search regions for PI gains are set to be $[0, 1]$ and the objective function is $'Minimize : ITAE_{min} = \int_0^{100s} t(|ACE_1| + |ACE_2|)dt'$.

Firstly, for every controller, MEDRs of every area of the system with 40% IR are calculated via Theorem 1 with sampling period $h = 5s$. The results are listed in Table 4. As can be seen from these results, K_8 has a larger EDR and is able to provide faster frequency response for power systems after a load-generation imbalance. Then, the system is tested in wind penetration levels with 40% IR under sampling period $h = 5s$ and is controlled by K_8 and other three discrete PI controllers, respectively. Frequency responses of area 1 are shown in Fig. 10 when the system is subjected to step changes $\Delta P_{w-1} = 0.02pu$ and $\Delta P_{w-2} = 0.05pu$ of wind power deviation (for $t \geq 0$). From Fig. 10, K_8 can restore the imbalance of load-generation in a shorter time about 13s, while K_{PI2} needs about 17s and K_{PI1} takes almost 32s. When the system is subjected to random changes of wind power deviation shown in Fig. 11, frequency responses of area 1 are shown in Fig. 12. It can be seen that K_8 still has better control performance than K_{PI2} and K_{PI1}. Based on the above results, it is not difficult to see that the proposed controller can ensure the power system operate stably in a larger sampling period. The proposed controller has better performance than not only manually adjusted PI controller, but also PSO-tuned PI controller. It shows the effectiveness and superiority of using EDR to guide the design of a fast secondary frequency controller.

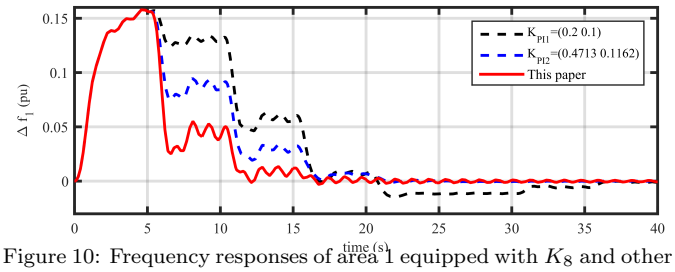

Figure 10: Frequency responses of area 1 equipped with K_8 and other three PI controllers under step changes of wind power deviation.

Table 4: MEDRs in every area of traditional two-area power systems under K_8, K_{PI1}, and K_{PI2}

	$K_8[this\ paper]$	$K_{PI2}[PSO]$	$K_{PI1}[manual]$
MEDRs	0.145	0.117	0.040

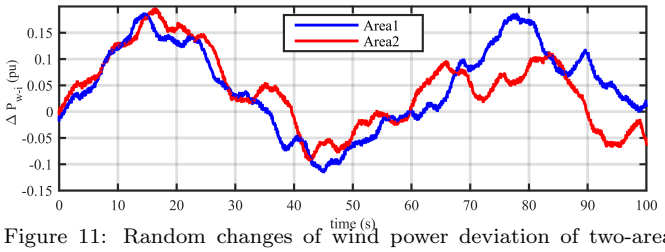

Figure 11: Random changes of wind power deviation of two-area power systems.

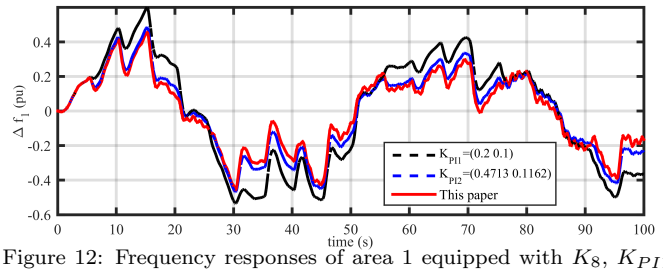

Figure 12: Frequency responses of area 1 equipped with K_8, K_{PI1} and K_{PI2} under random changes of wind power deviation.

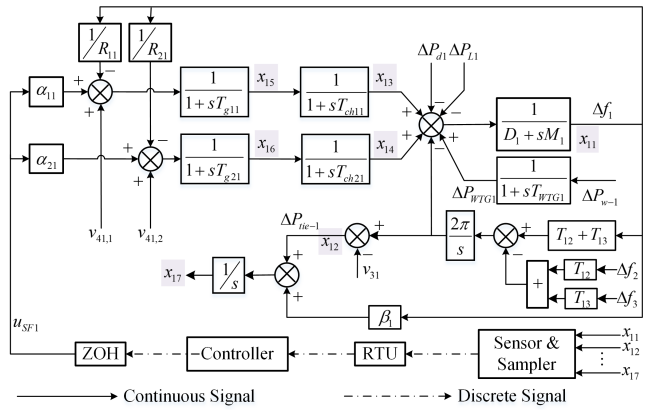

Figure 13: Detailed LFC model of area 1 of deregulated three-area LFC with wind power.

4.3. Deregulated three-area LFC with wind power

Assume that each area of the deregulated three-area power system includes two Gencos and two Discos, and transmission delays of control signal are all considered as 0.3s in three areas. The detailed linear system model of area 1 in three areas is shown in Fig. 13. Areas 2 and 3 are similar to area 1 and are omitted here due to limited space. Their detailed interaction structure is shown in Fig. 14, and their parameters with 30% IR are listed in Table 8 in appendix [10]. In the following controller design, the wind power is regarded as disturbance so as to compare the existing controllers in [23] and [10] under the same design system. Yet, in simulation, the wind power is introduced to restore the real environment and $T_{WTG} = 1.5s$.

4.3.1. Controller design

For a given $h = 3s$ of each area, controller K_{11} is developed by $\lambda_{min} = 0$, and $\lambda_{max} = 3$ and following the procedure in S2.1, and maximum EDRs 0.12, 0.25 and 0.25 are also obtained in three areas, respectively. K_{11} and the PID-type controllers K_{12} (reported in [23]) and K_{13} (reported in [10]) are shown in the Table 5.

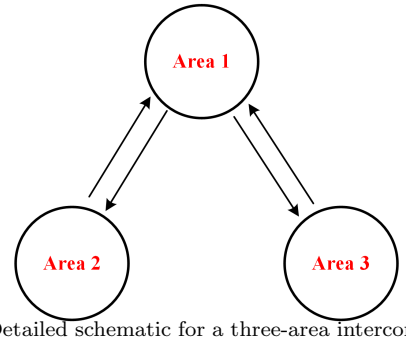

Figure 14: Detailed schematic for a three-area interconnected power systems.

4.3.2. Comparison and analysis

Firstly, for every controller, MEDRs of every area of the system with 30% IR are calculated via Theorem 1 with sampling period $h = 3s$, and MASPs of every area of the system with 30% IR are also derived with $\lambda = 0.1$. The results are listed in Table 5. 'NA' represents infeasibility. As can be seen from these results, when the sampling period is set to 3s, it can get a larger EDRs for K_{11} designed in this paper, which indicates that this controller can provide a faster frequency response than K_{12} and K_{13}. Also, when the EDR is set to 0.1, K_{11} can also make the power system operate in a larger sampling period. Compared with K_{11}, K_{12} has poor performance, while K_{13} can only work in smaller sampling period. Secondly, the system equipped with above three controllers operates in wind penetration level with 30% IR under sampling period $h = 3s$ and is tested in the following two scenarios with different disturbances.

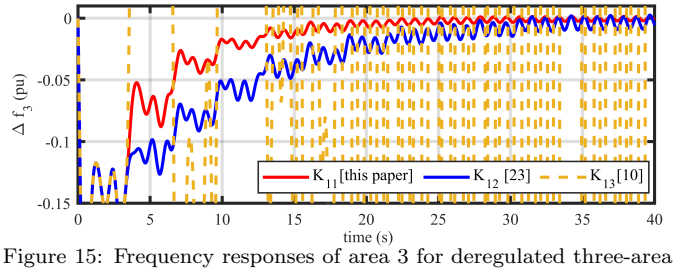

Figure 15: Frequency responses of area 3 for deregulated three-area power systems equipped with controllers K_{11}-K_{13} in scenario 1.

Scenario 1 [Load disturbance]: The system is subjected to step changes of load demands in three areas, i.e., $\Delta P_{d1} = 0.06pu$, $\Delta P_{d2} = 0.08pu$ and $\Delta P_{d3} = 0.1pu$ (for $t \geq 0$). Frequency responses of area 3 are shown in Fig. 15. The responses of areas 1 and 2 are similar and omitted here. Fig. 15 shows that K_{11} obtained can effectively suppress frequency deviation and recover the balance between generation and load within a shorter time (about 20s) than K_{12}, while K_{13} cannot generate effective actions to restore the balance.

Scenario 2 [Load and wind power deviation disturbances]: The system is tested in combination of Poolco and bilateral-based transactions based on parameters given in [23]. Assume that a step load of 0.1 pu is demanded by each Disco in three areas for $t \geq 0$; and Disco 1 in area 1 and area 2, and Disco 2 in area 3 demand 0.06 pu, 0.08 pu, and 0.1 pu as un-contracted loads for $t \geq 0$, respectively. Step changes of wind power deviation are $\Delta P_{wind1} = 0.06pu$, $\Delta P_{wind2} = -0.04pu$ and $\Delta P_{wind3} = 0.04pu$ for $t \geq 0$. Frequency responses of area 3 are shown in Fig. 16. The responses of areas 1 and 2 are similar and omitted here. From Fig. 16, similarly, K_{11} shows better performance in frequency response speed and suppression of frequency deviation than K_{12}, and K_{13} results in instability of

Table 5: Load frequency controllers, and their corresponding MASPs and MEDRs in every area of deregulated three-area power systems under different control schemes in [23], [10] and this paper.

Area	K_{11} [This paper]	MASPs(s)	MEDRs
1	-[0.0165 0.0076 0.0453 0.0425 0.0084 0.0113 0.1417]	7.10	0.144
2	-[0.0378 0.0255 0.0796 0.0850 0.0145 0.0175 0.2650]	4.82	0.276
3	-[0.0289 0.0387 0.0823 0.0904 0.0202 0.0148 0.2651]	4.82	0.276
Area	K_{12}[23]	MASPs(s)	MEDRs
1	-[-0.0473 0.1456 0.0137]	0.43	0.043
2	-[-0.0361 0.1233 0.0483]	3.42	0.118
3	-[0.0779 0.1040 0.0259]	4.10	0.102
Area	K_{13}[10]	MASPs(s)	MEDRs
1	-[0 0.9 0.4]	0.14	NA
2	-[0.1 0.8 0.3]	0.38	NA
3	-[0.8 0.9 0.9]	0.16	NA

frequency.

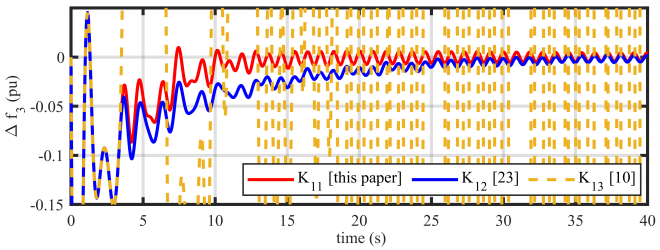

Figure 16: Frequency responses of area 3 for deregulated three-area power systems equipped with load frequency controllers K_{11}-K_{13} in scenario 2.

Based on the above mathematical analysis and simulation results, it demonstrates that the controller, which is designed in continuous mode and then used by the ZOH in the power system, will degrade performance and even cause instability. The controller designed in this paper can ensure the operation of the system under a larger sampling period. This conclusion is the same as the results of the above two cases. Moreover, compared with the robust LFC scheme, the proposed LFC scheme designed by EDR in this paper has a faster frequency response speed. It shows the effectiveness and superiority in dealing with the problem of the faster frequency response and bigger frequency deviation due to the reduced inertia of power system.

Remark 4. As can be seen from Figs. 10, 15 and 16, due to the periodic update of the control signal, the frequency deviation of the power system cannot be suppressed after the disturbance and before the control signal takes effect. In particular, when the sampling period is larger, this phenomenon is more obvious. This is a drawback of discrete LFC scheme.

Remark 5. In order to reduce the communication burden, this paper adopts the method of increasing the sampling period to reduce the update times of measurements and control signals of power system. As for the small sampling period, the method proposed in this paper will not be adequate and scholars have applied the event-triggered control strategy to solve this problem [36, 37, 38]. If the sampling period can be enlarged, the method proposed in this paper is more appropriate due to its simple implementation. Also, the proposed method can provide the upper bound of the sampling period of the system under different controllers to guide the selection of the sampling period. Moreover, inspired from the event-triggered control scheme, if this scheme can be used under a larger sampling period, it is expected to further reduce the communication burden. This will be our future research.

Remark 6. Due to the large-scale of real power system and the availability of lab facility, it is difficult to carry out the experimental test of the proposed controller on a real power system. Thus, most current studies of power systems control usually employ numerical simulation tests of the designed controller on some benchmark power systems [10]-[33]. To demonstrate the effectiveness of the proposed LFC scheme, this paper has already carried out simulation studies on three case studies, which are widely for the LFC studies [8, 10, 18]. On the other side, the proposed controller has relatively simple state-feedback control law, and thus there are no difficulties in hardware implementation. In the future studies, hardware-in-loop test can be carried out to verify the feasibility of the proposed LFC scheme for the real power systems. In this test, the controller will be implemented at hardware dSpace platform (1104), and the real power system will be simulated based on dSpace platform (1006) or Real-time Digital Simulator (RTDS) platform. Moreover, the open communication network will also be simulated in-the-loop based on dSpace platform. This test will investigate the implementation feasibility of the proposed control method, and be our future research.

5. Conclusion

A discrete load frequency control scheme has been investigated for power systems with high penetration of wind power based on sampled-data control. The proposed scheme can operate in a larger sampling period so as to reduce communication burden. Moreover, to deal with faster frequency response and larger frequency deviation resulting from reduced inertia of power system due to high penetration of wind power, exponential decay rate as a new performance index has been introduced to guide the design of load frequency control with desired faster frequency speed. According to different requirements of sampling period and exponential decay rate, the controllers have been derived by presetting the sampling period and maximizing exponential decay rate, or by presetting exponential decay rate and maximizing sampling period. The feasibility of the load frequency control design can be evaluated by comparing the requirements with the preset values and the obtained maximums. The simulation results based on one-area power system, traditional two-area and deregulated three-area power system with wind power have validated the discrete load frequency control design.

Appendix

The detailed elements of the matrices Ψ_{1i} and Ψ_{2i} in (9) and (10) are shown as follows

$$\begin{aligned}
\Xi_{1i} &= Sym\left(e_1^T P_{1i} e_3 - e_2^T N_{2i}\Pi_2 + \Upsilon^T L_i(e_1 - e_2)\right) \\
&\quad - \Pi_1^T \begin{bmatrix} X_i & N_{1i} \\ * & V_i \end{bmatrix} \Pi_1 - \tfrac{1}{h}\Pi_2^T R_{3i}\Pi_2 + \Gamma_i \\
\Gamma_i &= Sym\left(\Pi^T M_i(e_3 - (A+\lambda I)e_1 - \rho_i B K_{SF} e_2)\right) \\
\Xi_{2i} &= e_3^T R_{1i} e_3 + \Pi_4^T \begin{bmatrix} R_{2i} & N_{2i} \\ * & R_{3i} \end{bmatrix} \Pi_4 + \Omega, \rho_1 = 1, \rho_2 = e^{\lambda h} \\
\Omega &= Sym\left(\Pi_1^T \begin{bmatrix} X_i & N_{1i} \\ * & V_i \end{bmatrix} \Pi_3\right), r = |x_i|,\ j = 1,2,3,4 \\
e_j &= \left[0_{r\times(j-1)r}, I_r, 0_{r\times(4-j)r}\right], Sym(\mathbb{A}) = \mathbb{A} + \mathbb{A}^T \\
\Pi &= \left[e_1^T, e_2^T, e_3^T\right]^T, \Upsilon = [\Pi^T, e_4^T]^T, \Pi_1 = \left[e_1^T, e_2^T, e_4^T\right]^T \\
\Pi_2 &= \left[e_4^T, e_1^T - e_2^T\right]^T, \Pi_3 = \left[e_3^T, 0, e_1^T\right]^T, \Pi_4 = \left[e_2^T, e_1^T, e_3^T\right]^T.
\end{aligned}$$

The system parameters used in the simulations are reported in Tables 6-8 below.

Table 6: Parameters for LFC scheme of one-area power systems

D	M	R	T_g	T_{ch}
0.0830 pu/Hz	0.1667 pu·s	2.40 Hz/pu	0.08 s	0.30s

References

[1] P. Kundur. *Power System Stability and Control*. New York: Mc Graw Hill, 1994.

[2] A. Kumar, O. P. Malik. "Discrete analysis of load-frequency control problem," *IEE Proc. C-Gener. Transm. Distrib.*, vol. 131, no. 4, pp. 144-145, 1984.

[3] H. Bevrani. *Robust Power System Frequency Control*. New York: Springer, 2014.

[4] J. Moccia, A. Arapogianni, J. Wilkes, C. Kjaer, R. GruetPure, S. Azau, J. Scola, A. Zervos. "Power-wind energy targets for 2020 and 2030," *Eur. Wind Energy Assoc.*, Technical Report, July 2011.

[5] S. Liao, W. Yao, X. Han, J Wen, S. Cheng. "Chronological operation simulation framework for regional power system under high penetration of renewable energy using meteorological data," *Appl. Energy*, vol. 203, pp. 816-828, Oct. 2017.

[6] S. K. Pandey, S. R. Mohanty, N. Kishor. "A literature survey on load-frequency control for conventional and distribution generation power systems," *Renew. Sust. Energ. Rev.*, vol. 25, no. 5, pp. 318-334, Sept. 2013.

[7] R. Yan, T. K. Saha, N. Modi, N. A. Masood, M. Mosadeghy. "The combined effects of high penetration of wind and PV on power system frequency response," *Appl. Energy, vol. 145, pp. 320-330, May 2015.*

[8] N. Nguyen, J. Mitra. "An analysis of the effects and dependency of wind power penetration on system frequency regulation," IEEE Trans. Sust. Energy, vol. 7, no. 1, pp. 354-363, Jan. 2016.

[9] Enhanced Frequency Response, Nat. Grid, 2016. Available: https://www.nationalgrideso.com/balancing-services/frequency-response-services/enhanced-frequency-response-efr.

[10] H. Shayeghi, A. Jalili, H. A. Shayanfar. "Robust modified GA based multi-stage fuzzy LFC," Energy Convers. Manage., vol. 48, no. 5, pp. 1656-1670, May 2007.

[11] C. Peng, J. Li, M. Fei. "Resilient event-triggering H_∞ load frequency control for multi-area power systems with energy-limited DoS attacks," IEEE Trans. Power Syst., vol. 32, no. 5, pp. 4110-4118, Sept. 2017.

[12] P. Dahiya, P. Mukhija, A. R. Saxena. "Design of sampled data and event-triggered load frequency controller for isolated hybrid power system," Int. J. Electr. Power Energ. Syst., vol. 100, pp. 331-349, Sept. 2018.

[13] Y. Wang, R. Zhou, C. Wen. "Robust load-frequency controller design for power systems," IEE Proc. Part C, vol. 140, no. 5, pp. 11-16, Jan. 1993.

[14] Y. Wang, R. Zhou, L. Gao. "H_∞ controller design for power system load frequency control," Proc. IEEE TENCON, pp. 68-71, 1993.

[15] Z. Q. Wang, M. Sznaier. "Robust control design for load frequency control using μ-synthesis," Conf. Record Southcon. IEEE, pp. 186-190, 1994.

[16] M. Azzam. "Robust automatic generation control," Energy Convers. Manage., vol. 40, no. 13, pp.1413-1421, Sep. 1999.

[17] H. Bevrani, M. R. Feizi, S. Ataee. "Robust frequency control in an islanded microgrid: H_∞ and μ-Synthesis approaches," IEEE Trans. Smart Grid, vol. 7, no. 2, pp. 706-717, March, 2016.

[18] W. Tan, Z. Xu. "Robust analysis and design of load frequency controller for power systems," Electric Power Syst. Res., vol. 79, no. 5, pp. 846-853, May 2009.

[19] H. Shayeghi, H. A. Shayanfar, A. Jalili. "Multi-stage fuzzy PID power system automatic generation controller in deregulated environments," Energy Convers. Manage., vol. 47, no. 18-19, pp. 2289-2845, NOv. 2006.

[20] W. Tan. "Unified tuning of PID load frequency controller for power systems via IMC," IEEE Trans. Power Syst., vol. 25, no. 1, pp. 341-350, Feb. 2010.

[21] L. Jiang, W. Yao, Q. H. Wu, J. Y. Wen, S. J. Cheng. "Delay-dependent stability for load frequency control with constant and time-varying delays," IEEE Trans. Power Syst., vol. 27, no. 2, pp. 932-941, May 2012.

[22] C. K. Zhang, L. Jiang, Q. H. Wu, Y. He, M. Wu. "Further results on delay-dependent stability of multi-area load frequency control," IEEE Trans. Power Syst., vol. 28, no. 4, pp. 4465-4474, Nov. 2013.

[23] C. K. Zhang, L. Jiang, Q. H. Wu, Y. He, M. Wu. "Delay-dependent robust load frequency control for time delay power systems," IEEE Trans. Power Syst., vol. 28, no. 3, pp. 2192-

Table 7: Parameters of LFC scheme of traditional two-area power system with with %40 IR

D	M	R	T_g	T_{ch}	β	T_{WTG}	T_{12}
0.0150 pu/Hz	0.1000 pu·s	5.00 Hz/pu	0.08 s	0.40 s	0.2150 pu/Hz	1.5 s	0.200 pu/rad

Table 8: Parameters of LFC scheme of deregulated three-area power systems with %30 IR

	k-i: the k_{th} generator of area i							Control area		
	1-1	2-1	1-2	2-2	1-3	2-3		1	2	3
T_{ch}(s)	0.32	0.30	0.30	0.32	0.31	0.34	M (pu·s)	0.1500	0.1875	0.1440
T_g (s)	0.06	0.08	0.06	0.07	0.08	0.06	D(pu/Hz)	0.0084	0.0084	0.0080
R(Hz/pu)	2.67	2.78	2.78	3.00	3.11	2.67	β (pu/Hz)	0.4250	0.3966	0.3522
α	0.5	0.5	0.5	0.5	0.6	0.4	T_{ij}(pu/rad)	$T_{12} = 0.245$,$T_{13} = 0.212$,$T_{23} = 0$		

2201, Aug. 2013.

[24] L. Jin, C. K. Zhang, Y. He, L. Jiang, M. Wu. "Delay-dependent stability analysis of multi-area load frequency control with enhanced accuracy and computation efficiency," IEEE Trans. Power Syst., vol. 34, no. 5, pp. 3687-3696, Sept. 2019.

[25] S. Ali, G. Yang, C. Huang. "Performance optimization of linear active disturbance rejection control approach by modified bat inspired algorithm for single area load frequency control concerning high wind power penetration," ISA Trans., vol. 81, pp. 163-176, Oct. 2018.

[26] H. Bevrani, P. R. Daneshmand. "Fuzzy logic-based load-frequency control concerning high penetration of wind turbines," IEEE Syst. Jour., vol. 6, no. 1, pp. 173-180, March 2012.

[27] T. Hiyama. "Optimisation of discrete-type load-frequency regulators considering generation-rate constraints," IEE Proc. C-Gener. Transm. Distrib., vol. 129, no. 6, pp. 285, 1982.

[28] K. Vrdoljak, I. Petrovic, N. Peric. "Discrete-time sliding mode control of load frequency in power systems with input delay," Int. Power Electron. Motion Control Conf., pp. 567-572, 2006.

[29] X. Su, X. Liu, Y. D. Song. "Event-triggered sliding-mode control for multi-area power systems," IEEE Trans. Ind. Electron., vol. 64, no. 8, pp. 6732-6741, Aug. 2017.

[30] Y. Mi, X. Hao, Y Liu, Y. Fu, C. Wang, P. Wang, P. C. Loh. "Sliding mode load frequency control for multi-area time-delay power system with wind power integration," IET Generation, Transmission, Distribution, vol. 11, no. 18, pp. 4644-4653, June 2017.

[31] Y. Cui, L. Xu, M. Fei, Y. Shen. "Observer based robust integral sliding mode load frequency control for wind power systems," Control Eng. Pract., 2017, vol. 65, pp. 1-10, May 2017.

[32] Y. Zhang, D. Yue. "Digital PID based load frequency control through open communication networks," IEEE Control Decis. Conf., pp. 6243-6248, 2015.

[33] X. Liu, Y. Zhang, K. Y. Lee. "Coordinated distributed MPC for load frequency control of power system with wind farms," IEEE Trans. Ind. Electron., vol. 64, no. 6, pp. 5140-5150, June 2017.

[34] E. Fridman. "A refined input delay approach to sampled-data control," Automatica, vol. 46, pp. 421-427, Feb. 2010.

[35] X. C. ShangGuan, Y. He , L. Jiang. "Load frequency control in power systems via a sampled-data controller," 2018 37th Chinese Control Conf., IEEE, pp. 8940-8945, 2018.

[36] S. Wen, X. Yu, Z. Zeng, J. Wang. "Event-triggering load frequency control for multiarea power systems with communication delays," IEEE Trans. Ind. Electron., vol. 63, no. 2, pp. 1308-1317, Feb. 2016.

[37] L. Dong, Y. Tang, H. He, C. Sun. "An event-triggered approach for load frequency control with supplementary ADP," IEEE Trans. Power Syst., vol. 32, no. 1, pp. 581-589, Jan. 2017.

[38] C. Peng, J. Zhang, H. Yan. "Adaptive event-triggering H_∞ load frequency control for network-based power systems," IEEE Trans. Ind. Electron., vol. 65, no. 2, pp. 1685-1694, Feb. 2018.

[39] B. M. Gundogdu, S. Nejad, D. T. Gladwin, M. P. Foster, D. A. Stone. "A battery energy management strategy for U.K. enhanced frequency response and triad avoidance," IEEE Trans. Ind. Electron., vol. 65, no. 12, pp. 9509-9517, Dec. 2018.

[40] T. N. Pham, H. Trinh. "Load frequency control of power systems with electric vehicles and diverse transmission links using distributed functional observers," IEEE Trans. Smart Grid, vol.7, no. 1, pp. 238-252, Jan. 2016.

[41] H. Hui, Y. Ding, Y. Song, S. Rahman. "Modeling and control of flexible loads for frequency regulation services considering compensation of communication latency and detection error," Appl. Energy, vol. 250, pp. 161-174, 2019.

[42] D. Ochoa, S. Martinez. "Fast-frequency response provided by DFIG-wind turbines and its impact on the grid," *IEEE Trans. Power Syst.*, vol. 32, no. 5, pp. 4002-4011, Sept. 2017.

[43] M. Benidris, J. Mitra. "Enhancing stability performance of renewable energy generators by utilizing virtual inertia," IEEE Power Energ. Soc. Gen. Meeting, pp. 1-6, 2012.

[44] H. Jia, X. Li, Y. Mu, C. Xu, Y. Jiang, X. Yu, J. Wu, C. Dong. "Coordinated control for EV aggregators and power plants in frequency regulation considering time-varying delays," Appl. Energy, vol. 210, pp. 1363-1376, Jan. 2018.

[45] A. Seuret. "A novel stability analysis of linear systems under asynchronous samplings," Automatica, vol. 48, no. 1, pp. 177-182, Jan. 2012.

[46] K. Liu, E. Fridman. "Wirtinger's inequality and Lyapunov-based sampled-data stabilization," Automatica, vol. 48, no. 1, pp. 102-108, Jan. 2012.

[47] Q. Zhu, L. Jiang, W. Yao, C. K. Zhang, C. Luo. "Robust load frequency control with dynamic demand response for deregulated power systems considering communication delays," Electr. Power Compon. Syst., vol. 32, no. 1, pp. 75-87, Nov. 2016.